Geophys. J. Int. (2009) **178,** 638–650 doi: 10.1111/j.1365-246X.2009.04193.x

Generalized sampling interpolation of noisy gravity/gravity gradient data

James While,[1]* Ed Biegert[2] and Andrew Jackson[3]

[1]*School of Earth and Environment, University of Leeds, Leeds* LS2 9JT, *UK. E-mail: jwh@mail.nerc-essc.ac.uk*
[2]*Shell International Exploration and Production Inc, Bellaire Technology Center, Houston, Texas, USA*
[3]*Institut für Geophysik, ETH, Zürich, Switzerland*

Accepted 2009 March 26. Received 2009 March 20; in original form 2008 October 3

SUMMARY

The generalized sampling expansion (GSE) has been shown as a method for successfully interpolating combined gravity and gravity gradient data sets when the data are undersampled. The presence of noise on data sets renders such interpolation more difficult and many applications (known as expansions) of the GSE can be shown to intolerably amplify noise. However, many key expansions can be shown to successfully interpolate noisy data and even, given limited gradient error and sufficiently narrow line-spacing, reduce noise. These results can be shown to hold for both random noise and along-line correlated (levelling error type) noise. Unfortunately, the only expansion capable of interpolating a data set sampled at $3\times$ conventional line-spacing, the Three-rectangle expansion, has a poor noise response and always acts to amplify data error. The GSE method bares up well against other methods of gradient enhanced interpolation; in numerical tests several expansions for the gravity field produce less noisy output than any of the pseudo-line, gradient enhanced minimum curvature or gradient enhanced Akima spline methods. Despite edge effects and using only gradient data with no gravity component, the GSE applied to real undersampled survey data bares up well against conventional interpolation, reducing noise where the data are clearly undersampled.

Key words: Image processing; Fourier analysis; Gravity anomalies and Earth structure.

INTRODUCTION

Since the mid-1990s gravity gradiometry has become a practical exploration tool in the geophysicist's arsenal (Bell *et al.* 1997). Unaffected by linear accelerations of the measuring instrument, gravity gradients tend, especially at short wavelengths, to have higher signal-to-noise ratios than direct gravity measurements (Pratson *et al.* 1998), and thus potentially allow us to probe the subsurface in much greater detail. Most commercial gradiometers measure either the full gradient tensor (Murphy 2004), which has five independent components, or a reduced subset of elements derived from this tensor (Dransfield & Lee 2004). Thus there has been significant effort into combining multiple measured gradients together, sometimes with gravity, for data inversions (Vasco 1989; Vasco & Taylor 1991; Zhdanov *et al.* 2004; Droujinine *et al.* 2007), full tensor interpolation (FitzGerald & Holstein 2006), tensor deconvolution (Mikhailov *et al.* 2007) and noise detection and reduction (While *et al.* 2006; Pajot *et al.* 2008). Of particular relevance to this paper, it is shown in While *et al.* (2008, hereafter WBJ08) that undersampled measurements of gravity gradients and gravity can be combined together to obtain accurate, aliasing free, interpolations of gravity or gravity gradient data.

In summary, WBJ08 discusses the application in two dimensions of the generalized sampling expansion (GSE; Papoulis 1977) to idealized noise free gravity/gravity gradient data. In principle, given band-limited data of infinite extent, the GSE is a method that can perfectly reproduce the true gravity/gradient field from undersampled data. The method is applicable to all gravity (or indeed magnetic) gradient data sampled in a periodic manner, though the sampling does not need to be rectangular. Given a geophysical survey consisting of equispaced parallel data-lines that are undersampled in the cross-line direction the GSE proceeds as follows. First, the undersampled data are Fourier transformed into the spectral domain. Once this is done a linear matrix equation is written that relates the multiple gravity/gradient

*Now at: ESSC, University of Reading, Leeds, UK.

Table 1. The minimum and maximum variances of the successful sampling expansions calculated numerically using eq. (10).

Expansion geometry	Output component	Input components	min σ^2	max σ^2
Three-rectangle	U_z	$\{\tilde{U}_z, \tilde{U}_{yz}, U_{zz}\}$	1	4.43
Two-rectangle(A)	U_z	$\{\tilde{U}_z, \tilde{U}_{yz}\}$	0.43	1
Two-rectangle(B)	U_{zz}	$\{\tilde{U}_z, \tilde{U}_{yz}\}$	2.17	9.14
Two-rectangle(C)	U_{zz}	$\{\tilde{U}_{zz}, \tilde{U}_{yz}\}$	1	1.9
Two-rectangle(D)	U_{xz}	$\{\tilde{U}_{xz}, \tilde{U}_{xy}\}$	1	1.9
Two-rectangle(E)	U_{yz}	$\{\tilde{U}_{yy}, \tilde{U}_{yz}\}$	1	1.9
Four-square	U_z	$\{\tilde{U}_z, \tilde{U}_{xz}, \tilde{U}_{yz}, \tilde{U}_{xy}\}$	0.43	1
Four-hexagon(A)	U_z	$\{\tilde{U}_z, \tilde{U}_{xx}, \tilde{U}_{xz}, \tilde{U}_{yz}\}$	0.43	1.70
Four-hexagon(B)	U_z	$\{\tilde{U}_z, \tilde{U}_{yy}, \tilde{U}_{xz}, \tilde{U}_{yz}\}$	0.48	1.77
Four-hexagon(C)	U_z	$\{\tilde{U}_z, \tilde{U}_{xx} - \tilde{U}_{yy}, \tilde{U}_{xz}, \tilde{U}_{yz}\}$	0.44	1
Four-hexagon(D)	U_z	$\{\tilde{U}_z, \tilde{U}_{zz} - \tilde{U}_{xx}, \tilde{U}_{xz}, \tilde{U}_{yz}\}$	0.48	3.50
Three-hexagon(A)	U_z	$\{\tilde{U}_z, \tilde{U}_{xz}, U_{yz}\}$	0.57	1
Three-hexagon(B)	U_{zz}	$\{\tilde{U}_{zz}, \tilde{U}_{xz}, U_{yz}\}$	1	4.3
Three-hexagon(C)	U_{zz}	$\{\tilde{U}_{yy} - \tilde{U}_{zz}, \tilde{U}_{xz}, U_{yz}\}$	0.8	5.1

Note: In all cases the covariances of the input data are assumed zero with all the variances set equal to one. The output variances are given in arbitrary units.

spectra to the spectra of a single 'true' gravity or gradient field. The true field is then found by solving the matrix equation and inverse transforming back into the space domain. Depending on the sampling, the desired output, and the gradient components available, there are many methods, termed 'expansions', of applying the GSE to gravity data. WBJ08 discusses several expansions, most of which are listed in Table 1, the theoretically most powerful of which can find the true field from data sampled at treble normal line-spacing. However, WBJ08 shows that such ideal results cannot be realized due to edge effects and because gravity data are never band-limited, both of which are discussed in detail. Despite these effects it is shown that some expansions can effectively double the minimum line-spacing required to sample a gravity field, which has significant implications for designing sparser, lower cost gradient surveys. However, within WBJ08 the effects of signal noise are neglected and the only examples given are from ideal noise free data. This paper seeks to address this issue and examines how noise, both random and along-line correlated (i.e. levelling error), affects the GSE. In presenting this paper, we show that several expansions are well behaved under the addition of both random and along-line correlated noise. These results are of crucial importance because an expansion is of no practical value if it acts to intolerably amplify noise.

Discussions within the literature on the GSE applied to noisy data have, mostly, been confined to determining conditions under which expansions of noisy data have unbounded variance; in such circumstances an expansion is said to be ill-posed. Cheung & Marks (1985); Brown & Cabrera (1990, 1991) discuss, in 1-D, the circumstances under which the GSE is well-posed. It is shown that the GSE is well-posed if $0 < |\det[\mathbf{H}(\mathbf{k})]| < \infty$, where $\mathbf{H}$ is the expansion matrix (described below in eq. 1), and $\mathbf{k}$ is the wavevector. Again in 1-D, Seidner & Feder (1998) compares the noise sensitivity of the GSE with conventional sampling, when both are sufficiently undersampled that they can only just reconstruct a signal. Provided all input components to the GSE are contaminated with equal noise, then it is shown that the variance of the output noise of the GSE is always greater than or equal to the variance of the noise using conventional sampling. The formulation of the optimal expansion matrix $\mathbf{H}$ (defined so as to produce the minimum square error) for this system is discussed in both Seidner & Feder (1998) and Seidner & Feder (1999). However, the study presented in the preceding references does not answer important questions about the GSE applied to noisy 2-D gravity/gradient data. For gravity/gradient data the variances of the measured gradient/gravity components are unlikely to be equal; this is especially true between gravity measurements and gradient measurements. Additionally, because of the method of operation of many gradiometers (see Lee 2001; Murphy 2004), the covariances between the individual gravity/gradient components are almost certainly non-zero. Therefore, for expansions of gravity/gradient data we must consider noise that is described by an arbitrary covariance matrix $\mathbf{C}_\mathrm{d}$.

Throughout this manuscript we will assume familiarity with the study presented in WBJ08, briefly summarized above, on the underlying theory of the GSE and its application—descriptions of the various expansions discussed below, which are listed in Table 1, can be found there. We also attempt, as far as possible, to follow the notation of WBJ08; in particular we denote U_{ab} as the derivative of the gravitational potential U with respect to a and b, while $\tilde{U}_{ab}$ denotes a measurement of this quantity. With this in mind, in this paper we discuss the effects of both random noise and along-line correlated noise on the GSE expansions. We begin below by reintroducing the equation that describes the GSE and convert this equation into the space domain. The subsequent section then details the theory that describes the propagation of random noise through the expansions. For random noise many of the expansions discussed in WBJ08 are shown to be well behaved (an example is given using the Four-square expansion) and are even, under some circumstances, capable of reducing noise. These results are, unfortunately, not seen to hold with the Three-rectangle expansion, which is shown to dramatically amplify noise. We then discuss the effects of changing the sample-spacing in expansions of noisy data. In this more general case most of the expansions are shown to remain well behaved over a wide range of line-spacings. Along-line correlated noise, which is common in potential field data, is then discussed. The response of the expansions to along-line correlated noise is calculated numerically using Fourier series to generate a noise model. Again it is found that when subjected to along-line correlated noise the important expansions, excluding the Three-rectangle expansion, are well behaved and in some

cases noise reducing. Lastly we demonstrate the GSE by applying the Two-rectangle(C) expansion to a set of deliberately undersampled real data collected in the North Sea. The expansion of this data set, though notably affected by edge effect errors at its boundaries, successfully eliminates large interpolation errors that are due to undersampling.

THE GSE

As discussed in WBJ08, the GSE can be defined for any band-limited signal sampled out to infinity. A further requirement is that the signal is 'regularly' sampled; that is, the signal is sampled at positions that satisfy $\mathbf{x} = \mathbf{Vq}$, where in two-dimensions $\mathbf{x}$ is a 2-D position vector, $\mathbf{V}$ is a 2×2 'sampling matrix', and $\mathbf{q}$ is drawn from $\mathbb{Z}^2$. In practise most sampling uses a rectangular lattice and $\mathbf{V}$ is diagonal, but this is not required. Indeed, WBJ08 spends considerable time discussing hexagonal sampling, which is the type of sampling that forms the bases for the hexagonal expansions discussed both here and in WBJ08. Given the above, the GSE is defined (for a derivation please see WBJ08) in the spectral domain by the matrix equation

$$\mathbf{U}(\mathbf{k}) = \mathbf{H}^{-1}(\mathbf{k})\mathbf{g}(\mathbf{k}), \qquad \mathbf{k} \in \mathcal{W}_0, \tag{1}$$

where $\mathbf{k}$ is the wavevector, and $\mathbf{g}$ is a vector of the Fourier spectra of m sampled gravity/gradient fields. The solution to the GSE equation $\mathbf{U}$ is an m element vector whose elements are the piecewise sections of the spectra of the 'true' signal. The matrix $\mathbf{H}$ is the characteristic matrix of an expansion and describes how the energy of the true signal is aliased to become the elements of $\mathbf{g}$. All spectra within this equation are defined within the region $\mathcal{W}_0$, referred to as the primary Nyquist region, whose area is set by the sampling used to collect the data. In 1-D $\mathcal{W}_0$ is the region between the positive and negative Nyquist frequencies. For our purposes of analysing the noise response of the GSE it is useful to work in the space domain. To this end we introduce the vector (known as the modulation vector; Cheung *et al.* 1989)

$$\mathbf{b}(\mathbf{x}) = \begin{Bmatrix} 1 \\ \exp\left[2\pi i(\tilde{\mathbf{V}}\mathbf{p}_2)^{\mathrm{T}}\mathbf{x}\right] \\ \vdots \\ \exp\left[2\pi i(\tilde{\mathbf{V}}\mathbf{p}_m)^{\mathrm{T}}\mathbf{x}\right] \end{Bmatrix}, \tag{2}$$

where the superscript T denotes transposition and $\mathbf{x}$ is a position vector. The matrix $\tilde{\mathbf{V}} = \mathbf{V}^{\mathrm{T}^{-1}}$, termed the periodicity matrix, describes how the spectra in $\mathbf{g}$ repeat themselves over the spectral domain, where each repetition occupies one Nyquist region $\mathcal{W}$ of spectral space. Each of the m vectors $\tilde{\mathbf{V}}\mathbf{p}_m$, where each $\mathbf{p}_m$ is a specified element of $\mathbb{Z}^2$, points to the Nyquist regions of spectral space where an element of $\mathbf{U}$ needs to be shifted in order to piecewise construct the true signal. As an example of eq. (2), the Two-rectangle(A) expansion expands to the two Nyquist regions defined by $\mathbf{p}_1 = (0, 0)$ and $\mathbf{p}_2 = (0, 1)$; thus, given a line-spacing Δy, $\mathbf{b}$ has two elements, which are 1 and $\exp(-\pi i \Delta y^{-1}\mathbf{x})$ respectively. By construction $\mathcal{F}^{-1}[\mathbf{b}(\mathbf{x})\mathbf{U}(\mathbf{k})] = a(\mathbf{x})$, where $a(\mathbf{x})$ is the complete space domain solution to the GSE and $\mathcal{F}^{-1}[\gamma] = \int \gamma \exp(2\pi \mathbf{k}^{\mathrm{T}}\mathbf{x})\mathrm{d}^2\mathbf{k}$ is the 2-D inverse Fourier transform. Provided the function described by $\mathbf{U}$ is band-limited to the m Nyquist regions of an expansion, then left-hand multiplying eq. (1) by $\mathbf{b}^{\mathrm{T}}$ and inverse Fourier transforming, we find

$$a(\mathbf{x}) = \iint_{\mathcal{W}_0} \mathbf{b}^{\mathrm{T}}(\mathbf{x})\mathbf{H}^{-1}(\mathbf{k})\mathbf{g}(\mathbf{k}) \exp(2\pi \mathbf{k}^{\mathrm{T}}\mathbf{x})\mathrm{d}^2\mathbf{k}; \tag{3}$$

note that $\mathbf{b}(\mathbf{x})$ does not depend on $\mathbf{k}$ and may be taken outside the double integral. Applying the convolution theorem of Fourier transforms, the above formula can be written as

$$a(\mathbf{x}) = |\det(\mathbf{V})| \sum_{\mathbf{q}\in\mathbb{Z}^2} \mathbf{b}^{\mathrm{T}}(\mathbf{x})\bar{\mathbf{H}}^{-1}(\mathbf{x} - \mathbf{Vq})\mathbf{d}(\mathbf{Vq}), \tag{4}$$

where $\bar{\mathbf{H}}^{-1} = \bar{F}^{-1}[\mathbf{H}^{-1}]$, $\mathbf{d}(\mathbf{Vq}) = \bar{F}^{-1}[\mathbf{g}(\mathbf{k})]$ is the data vector in the space domain, and the $|\det(\mathbf{V})|$ multiplication factor ensures equality in the total power between the space and spectral domains. In the above equation we have written the convolution explicitly as a sum as this simplifies the following derivations.

RANDOM NOISE

Real data are always subject to a degree of noise and in this section we consider the effect that random noise of zero mean has on the GSE. We can model random noise as a linear addition to ideal noise free data, that is,

$$\tilde{\mathbf{d}}(\mathbf{x}) = \mathbf{d}(\mathbf{x}) + \boldsymbol{\varepsilon}(\mathbf{x}), \tag{5}$$

where $\tilde{\mathbf{d}}$ are the noise contaminated data and $\boldsymbol{\varepsilon}$ is a vector, the same size as $\mathbf{d}$, of zero mean random noise. Substituting $\tilde{\mathbf{d}}$ for $\mathbf{d}$ in the space domain GSE, eq. (4), we get

$$\tilde{a}(\mathbf{x}) = |\det(\mathbf{V})| \sum_{\mathbf{q}\in\mathbb{Z}^2} \mathbf{b}^{\mathrm{T}}(\mathbf{x})\bar{\mathbf{H}}^{-1}(\mathbf{x} - \mathbf{Vq})\left[\mathbf{d}(\mathbf{Vq}) + \boldsymbol{\varepsilon}(\mathbf{Vq})\right], \tag{6}$$

where we have added a tilde above a to indicate that the expansion is now a noise contaminated estimate of the true function. Because we are modelling the noise as a linear addition, the first term in this equation is simply the regular noise free GSE and it is only the second term that contributes to the output noise. Therefore, if we denote the output error as $\bar{\varepsilon}$, we can write

$$\bar{\varepsilon}(\mathbf{x}) = |\det(\mathbf{V})| \sum_{\mathbf{q}\in\mathbb{Z}^2} \mathbf{b}^{\mathrm{T}}(\mathbf{x})\bar{\mathbf{H}}^{-1}(\mathbf{x}-\mathbf{V}\mathbf{q})\boldsymbol{\varepsilon}(\mathbf{V}\mathbf{q}). \tag{7}$$

Now, as the elements of $\boldsymbol{\varepsilon}$ are statistical quantities of zero mean, so $\bar{\varepsilon}$ must also be of zero mean. Therefore, the output noise of the GSE will be characterized by the variance (σ^2) of $\bar{\varepsilon}$. The variance is simply the expectation of the square of $\bar{\varepsilon}$, so

$$\sigma^2(\mathbf{x}) = |\det(\mathbf{V})|^2 \mathbf{b}^{\mathrm{T}}(\mathbf{x}) \left\{ \sum_{\mathbf{q}\in\mathbb{Z}^2} \sum_{\mathbf{q}'\in\mathbb{Z}^2} \bar{\mathbf{H}}^{-1}(\mathbf{x}-\mathbf{V}\mathbf{q}) \mathrm{E}\left[\boldsymbol{\varepsilon}(\mathbf{V}\mathbf{q})\boldsymbol{\varepsilon}^{\mathrm{T}}(\mathbf{V}\mathbf{q}')^*\right] \bar{\mathbf{H}}^{-1^{\mathrm{T}}}(\mathbf{x}-\mathbf{V}\mathbf{q}')^* \right\} \mathbf{b}(\mathbf{x})^*, \tag{8}$$

where the raised asterisk denotes complex conjugation and E denotes the expectation operator. If we assume the errors to be statistically stationary, then we can write $\mathrm{E}[\boldsymbol{\varepsilon}(\mathbf{V}\mathbf{q})\,\boldsymbol{\varepsilon}^{\mathrm{T}}(\mathbf{V}\mathbf{q}')^*] = \mathbf{C}_{\mathrm{d}}\delta_{\boldsymbol{q}\boldsymbol{q}'}$, where $\mathbf{C}_{\mathrm{d}}$ is the covariance matrix of the errors contained within $\boldsymbol{\varepsilon}$, and $\delta_{\boldsymbol{q}\boldsymbol{q}'}$ is the 2-D Kronecker delta. Making this substitution we obtain the error equation for stationary random noise in the GSE

$$\sigma^2(\mathbf{x}) = |\det(\mathbf{V})|^2 \mathbf{b}^{\mathrm{T}}(\mathbf{x}) \left[\sum_{\mathbf{q}\in\mathbb{Z}^2} \bar{\mathbf{H}}^{-1}(\mathbf{x}-\mathbf{V}\mathbf{q})\mathbf{C}_{\mathrm{d}}\bar{\mathbf{H}}^{-1^{\mathrm{T}}}(\mathbf{x}-\mathbf{V}\mathbf{q})^* \right] \mathbf{b}(\mathbf{x})^*. \tag{9}$$

This equation—using Parseval's theorem and noting from WBJ08 that the GSE is defined only within the primary Nyquist region—can also be written as

$$\sigma^2(\mathbf{x}) = |\det(\mathbf{V})| \mathbf{b}^{\mathrm{T}}(\mathbf{x}) \left[\iint_{\mathcal{W}_0} \mathbf{H}^{-1}(\mathbf{k})\mathbf{C}_{\mathrm{d}}\mathbf{H}^{-1^{\mathrm{T}}}(\mathbf{k})^* \mathrm{d}^2\mathbf{k} \right] \mathbf{b}(\mathbf{x})^*. \tag{10}$$

Both of eqs (9) and (10) give a complete description of any expansion's response to stationary random noise. It is worth noting that, other than the errors being statistically stationary and having zero correlation length, we have made no assumptions about the form of the input errors, which may have non-zero covariances. Thus, $\mathbf{C}_{\mathrm{d}}$ can be any positive definite symmetric matrix, whose off-diagonal elements define the error covariances. Furthermore, while the input errors described by $\mathbf{C}_{\mathrm{d}}$ are statistically stationary, this is not true for the output errors whose variance depends on $\mathbf{x}$. This is due to the $\mathbf{x}$ dependence of $\mathbf{b}$. In fact, from its definition in eq. (2), it can be seen that $\sigma^2(\mathbf{x})$ periodically repeats itself from one sample point to the next along the principle directions of the sampling.

An insight into what the above noise equations tell us can be gleaned if we use the eigenvalue decomposition $\mathbf{H} = \mathbf{P}\boldsymbol{\Psi}\mathbf{P}^{-1}$, where $\mathbf{P}$ is a matrix whose columns are the eigenvectors of $\mathbf{H}$, and $\boldsymbol{\Psi}$ is a diagonal matrix of the eigenvalues. Substituting into eq. (10) and rearranging we get

$$\sigma^2(\mathbf{x}) = |\det(\mathbf{V})| \mathbf{b}^{\mathrm{T}}(\mathbf{x}) \left(\iint_{\mathcal{W}_0} \mathbf{P}\boldsymbol{\Psi}^{-1}\mathbf{P}^{-1}\mathbf{C}_{\mathrm{d}}\mathbf{P}^{-1^{\mathrm{T}}}\boldsymbol{\Psi}^{-1}\mathbf{P}^{\mathrm{T}} \mathrm{d}^2\mathbf{k} \right) \mathbf{b}(\mathbf{x})^*, \tag{11}$$

where, for brevity, we have omitted the $\mathbf{k}$ dependence of $\mathbf{P}$ and $\boldsymbol{\Psi}^{-1}$. Mathematically this can be viewed as a rotation of $\mathbf{C}_{\mathrm{d}}$ into a new coordinate frame defined by the eigenvectors in $\mathbf{P}^{-1}$. The covariances are then scaled by the eigenvalues in $\boldsymbol{\Psi}^{-1}$ before being rotated back by $\mathbf{P}$ and integrated across the primary Nyquist region. It can be seen, therefore, that the ultimate magnitude of the output errors of the GSE will depend on the magnitude of the eigenvalues of $\mathbf{H}$—small eigenvalues produce large errors; large eigenvalues produce small errors.

PREDICTED ERROR OF THE EXPANSIONS

The output errors of any expansion can be predicted using either eq. (9) or eq. (10). Let us now, and likewise for the other gradient components, use ε_z to denote random errors on $\tilde{U}_z$ and examine the expected output errors of the expansions. The solutions to the error equations for both the Four-square expansion and Three-rectangle expansion are given in Figs 1 and 2, respectively. These figures show the expected output variance when both the along-line Δx and interline Δy spacing equal 1, and for when different components of $\mathbf{C}_{\mathrm{d}}$ have unitary value. The results shown are illustrative of important features of the noise characteristics of the GSE. First, the figures show the non-stationarity of the output variance. The periodicity with $\mathbf{b}(\mathbf{x})$ is most readily apparent with the Four-square expansion (Fig. 1), where the error pattern is clearly periodic in two directions. These periodic patterns also vary with the type of input error. Most strikingly, the contribution to the output variance from the covariances can, in some regions, be negative. This may at first seem to be a problem with the theory. However, because $\mathbf{C}_{\mathrm{d}}$ is constrained to be symmetric positive definite and because the output variance is the sum of the contributions from each element of $\mathbf{C}_{\mathrm{d}}$, the total output variance is always positive. A careful examination of the figures also shows that the output variance at the original data points (black diamonds) is always unity. This must be true because in these expansions the GSE is constrained to the data value at the original sample locations. However, the figures show that away from the original data points (such as at the interpolation points indicated by the pink crosses) the two expansions behave very differently. In both cases the gradient induced error increases away from the original data points, but for the Four-square expansion a reduction is seen in the gravity ($\mathrm{E}[\varepsilon_z^2]$) induced error. Consequently, given sufficiently small gradient noise

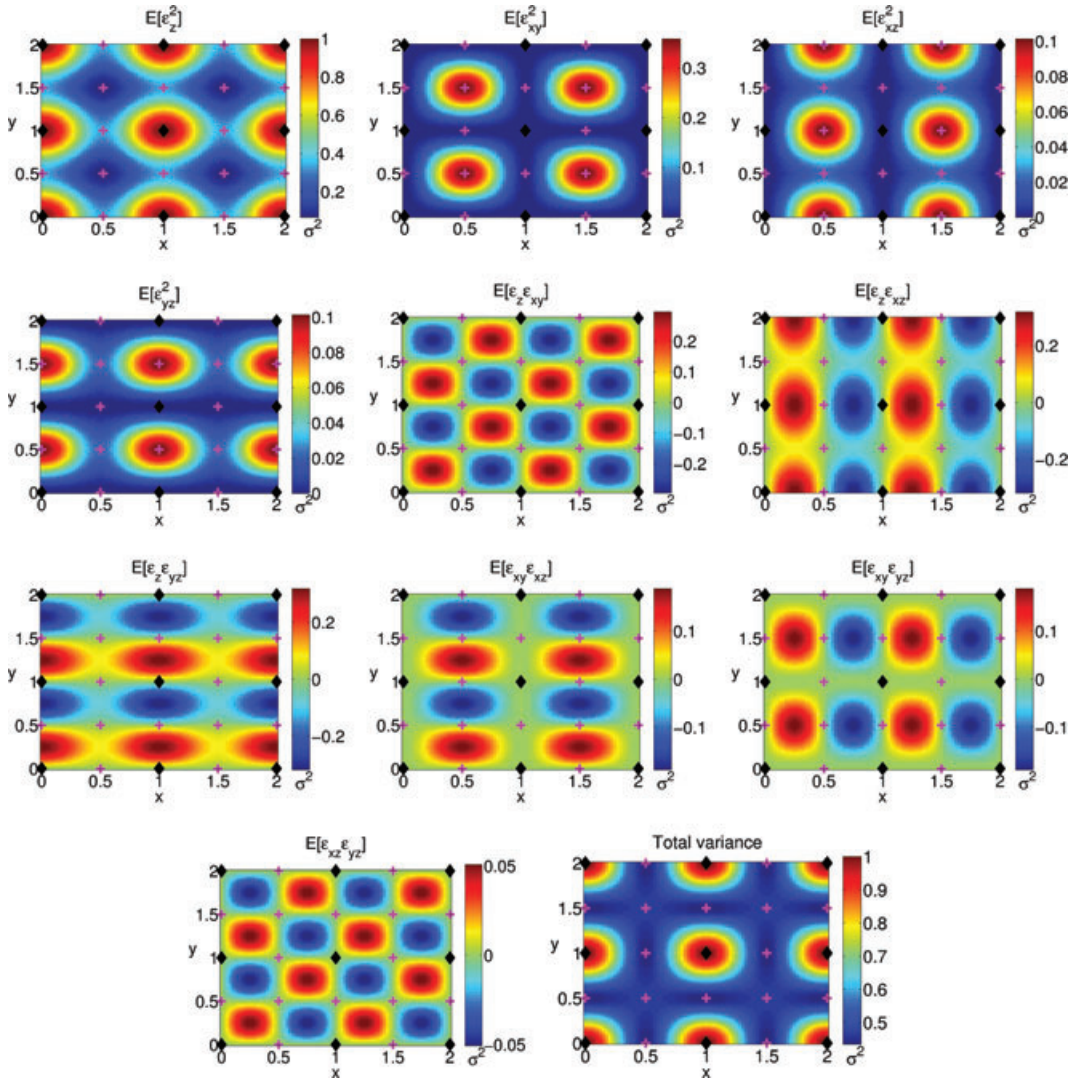

Figure 1. Output variance of the Four-square expansion. The images show the output variance due to each of the input variances and covariances. The total variance plot shows the sum of the four variance plots. In each case the input variance or covariance is taken as unity. The black diamonds mark the location of the input data points; pink crosses mark the locations of the output points of the expansion (assuming no zero padding in the spectral domain). All plots were calculated numerically using eq. (10).

(a constraint that cannot be considered separately from the line-spacing, see the next section) the error reduction from the gravity component will dominate and the Four-square expansion will reduce the noise. This is seen in the total variance plot in Fig. 1, where, for equivalent noise in all input components, the Four-square expansion is still seen to be noise reducing. As a result we regard the Four-square and similar noise-reducing expansions as well behaved under the addition of random noise. Conversely, in Fig. 2 we can see that for the Three-rectangle expansion the output variance is enhanced away from the original sample points for all of $\mathrm{E}[\varepsilon_z^2]$, $\mathrm{E}[\varepsilon_{zz}^2]$, and $\mathrm{E}[\varepsilon_{yz}^2]$. Consequently, any gravity field obtained using the Three-rectangle expansion will always be significantly more noisy than its inputs.

Figs 3 and 4 illustrate how the theoretical results shown in Figs 1 and 2 translate into actual noise on the output of the expansions. These figures show, respectively, the output of the Four-square and Three-rectangle expansions applied to a set of data contaminated with Gaussian noise. It is easily seen that the Four-square expansion has cleaned up the signal, while the Three-rectangle expansion has severely degraded it. The non-stationarity of the output is demonstrated in Fig. 3(d), which shows the output noise at the interpolation points of minimum variance (the pink crosses on the diagonal in Fig. 3).

We do not show the complete error variance plots of all possible expansions here. Instead, Table 1 lists the minimum and maximum output variance of several key expansions given unitary variance on each input component and zero covariances (i.e. $\mathbf{C}_\mathrm{d}$ is the identity matrix). Importantly, this table shows that the Two-rectangle(A) expansion, under the described circumstances, is a variance reducing expansion. This is a key result because WBJ08 shows that this expansion is the most useful of all of the expansions considered. However, it must be noted that a large number of the expansions in the table tend to amplify noise instead of reducing it.

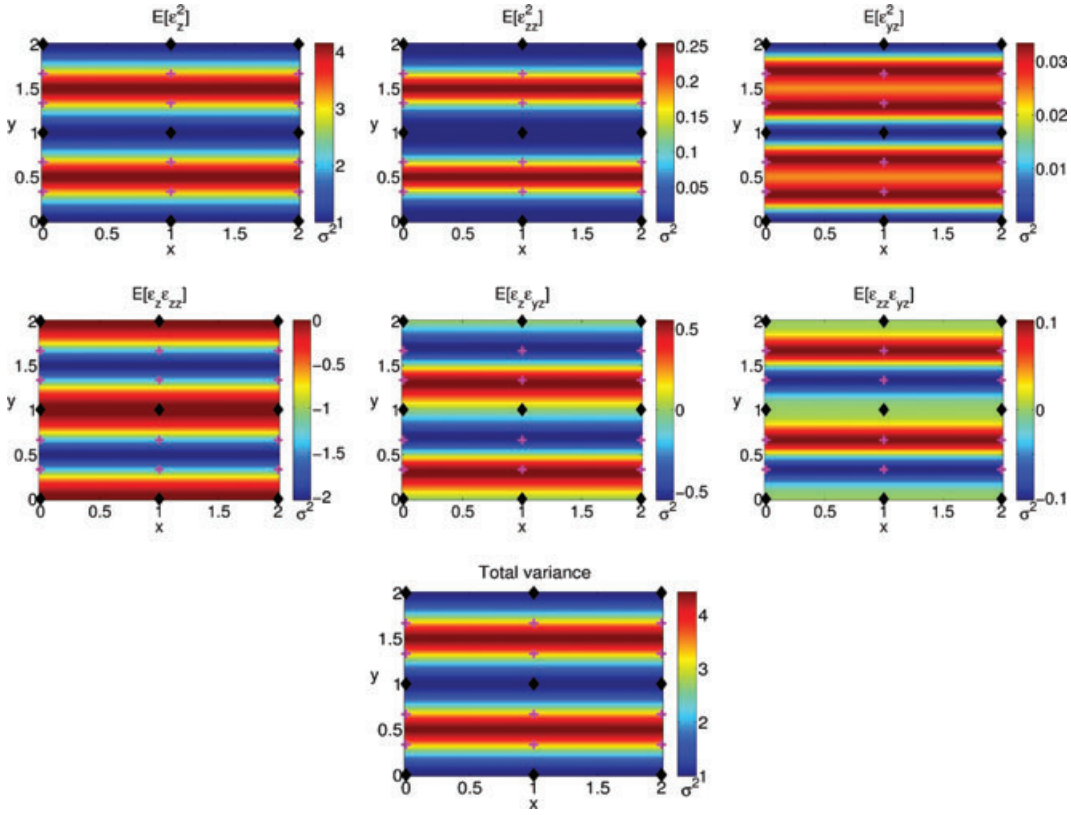

Figure 2. Output variance of the Three-rectangle expansion. The images show the output variance due to each of the input variances and covariances. The total variance plot shows the sum of the three variance plots. In each case the input variance or covariance is taken as unity. The black diamonds mark the location of the input data points; pink crosses mark the locations of the output points of the expansion (assuming no zero padding in the spectral domain). All plots were calculated numerically using eq. (10).

EFFECTS OF SAMPLE-SPACING

So far we have not considered sample-spacing in our evaluation of $\sigma^2(\mathbf{x})$. In fact, information about the sample-spacing is implicitly included within $\mathbf{H}(\mathbf{k})$, $\mathbf{V}$, and $\mathcal{W}_0$. However, the main reason for using the GSE is the interpolation of undersampled data; consequently it is of great interest to obtain an understanding of how changing the sample-spacing changes the output error of the expansions.

Our aim here is to relate the output noise of an expansion of arbitrary sample-spacing (Δx and Δy both of arbitrary value) to the output noise of an expansion where $\Delta x = \Delta y = 1$. Let us define a diagonal scaling matrix $\boldsymbol{\Upsilon}$ whose two diagonal elements (Υ_x and Υ_y) are scale factors in the x and y directions. Using this matrix any sampling matrix $\mathbf{V}$ can be related to its unscaled 'parent' $\mathbf{V}_\mathrm{u}$ by $\mathbf{V} = \boldsymbol{\Upsilon}\mathbf{V}_\mathrm{u}$. Using the inverse scale property of Fourier transforms, the wavevector $\mathbf{k}$ can be related to an unscaled wavevector $\bar{\mathbf{k}}$ by $\mathbf{k} = \boldsymbol{\Upsilon}^{-1}\bar{\mathbf{k}}$, which allows us to write the decomposition

$$\mathbf{H}(\mathbf{k}) = \boldsymbol{\Lambda}(\Upsilon_x, \Upsilon_y)\left[\mathbf{H}(\bar{\mathbf{k}}) + \mathbf{D}(\upsilon, \bar{\mathbf{k}})\right], \tag{12}$$

where $\upsilon = \frac{\Upsilon_y^2}{\Upsilon_x^2}$. As can be seen, when $\Upsilon_x \neq \Upsilon_y$ $\mathbf{H}$ is modified by the addition of a matrix $\mathbf{D}$ (here termed the distortion matrix). Furthermore, unless $\Upsilon_x = \Upsilon_y = 1$, $\mathbf{H}(\bar{\mathbf{k}})$ is also modified by multiplication with a diagonal matrix $\boldsymbol{\Lambda}$. These matrices, $\mathbf{D}$ and $\boldsymbol{\Lambda}$, represent different aspects of changing the sample-spacing: $\mathbf{D}$ describes the change in $\mathbf{H}$ due to the Nyquist regions distorting (stretching or compressing), while $\boldsymbol{\Lambda}$ describes the effect due to the change in area of the Nyquist regions. The forms of both $\mathbf{D}$ and $\boldsymbol{\Lambda}$ depend on the form of $\mathbf{H}$. In fact, for many expansions [such as the Two-rectangle(A) expansion] $\mathbf{D}$ can be shown to be always a zero matrix; it is only non-zero for expansions whose $\mathbf{H}$ matrices contain terms involving $(k_x^2 + k_y^2)$ (i.e. expansions that involve an integration or differentiation with respect to z). As an example of eq. (12) applied to a real expansion, we write it here in full for the Three-rectangle expansion

$$\begin{aligned}\mathbf{H}_{3\mathrm{r}}\left(\frac{\bar{k}_x}{\Upsilon_x}, \frac{\bar{k}_y}{\Upsilon_y}\right) = &\begin{pmatrix} 1 & 0 & 0 \\ 0 & \frac{2\pi}{\Upsilon_y} & 0 \\ 0 & 0 & \frac{2\pi i}{\Upsilon_y} \end{pmatrix} \left\{ \begin{bmatrix} 1 & 1 & 1 \\ a_1 & a_2 & a_3 \\ \bar{k}_y^2 & (\bar{k}_y+1)^2 & (\bar{k}_y-1)^2 \end{bmatrix} \right. \\ &\left. + \begin{bmatrix} 0 & 0 & 0 \\ \sqrt{\upsilon\bar{k}_x^2 + \bar{k}_y^2} - a_1 & \sqrt{\upsilon\bar{k}_x^2 + (\bar{k}_y+1)^2} - a_2 & \sqrt{\upsilon\bar{k}_x^2 + (\bar{k}_y-1)^2} - a_3 \\ 0 & 0 & 0 \end{bmatrix} \right\},\end{aligned} \tag{13}$$

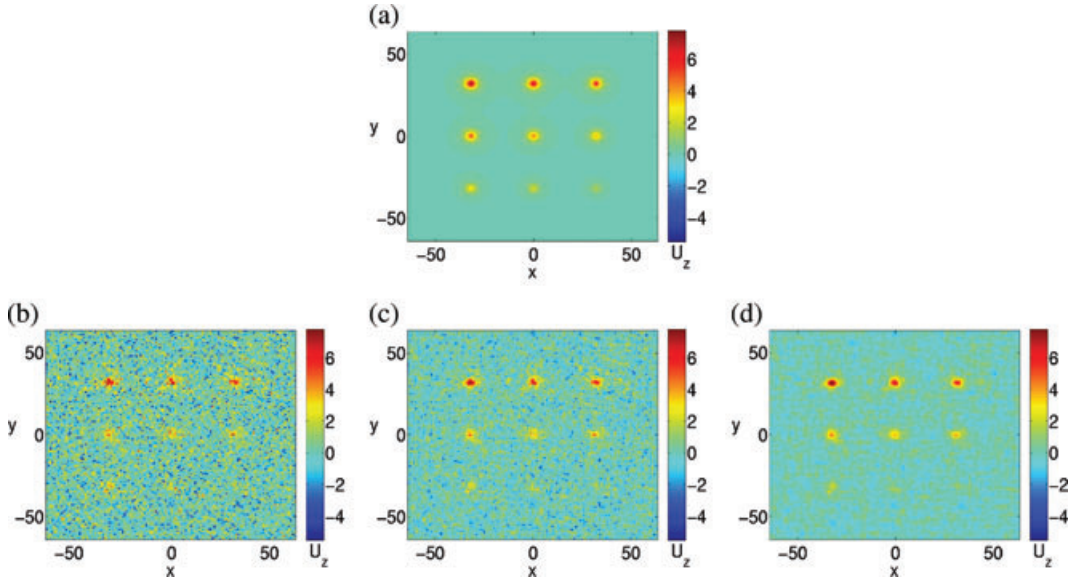

Figure 3. Four-square expansion of a noisy signal. (a) The test signal: gravity/gradient field of nine point sources of decreasing mass. The amplitude of the peaks decrease in decrements of 10 per cent. (b) Noise contaminated $\tilde{U}_z$ signal; all four gradient components are contaminated with Gaussian noise with a standard deviation of 20 per cent of the respective gravity/gradient peak amplitudes. (c) Four-square reconstruction of the noisy signal. (d) The reconstructed signal at the interpolation points of minimum variance (the pink crosses on the diagonal in Fig. 1).

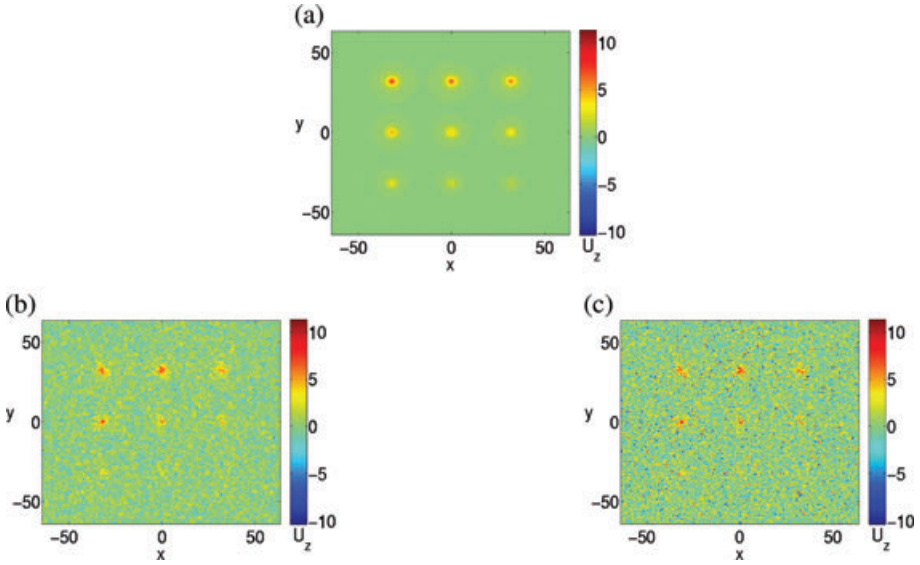

Figure 4. Three-rectangle expansion of a noisy signal. (a) The test signal: gravity/gradient field of nine points sources of decreasing mass. The amplitude of the peaks decrease in decrements of 10 per cent. (b) Noise contaminated $\tilde{U}_z$ signal; all three gradient components are contaminated with Gaussian noise with a standard deviation of 20 per cent of the respective gravity/gradient peak amplitudes. (c) Three-rectangle expansion of the noisy signal.

where a_1, a_2 and a_3 are $\sqrt{\bar{k}_x^2 + \bar{k}_y^2}$, $\sqrt{\bar{k}_x^2 + (\bar{k}_y + 1)^2}$ and $\sqrt{\bar{k}_x^2 + (\bar{k}_y - 1)^2}$, respectively, and the 2π and $2\pi i$ multiplication factors have been moved into the scaling matrix to shorten the equation.

By substituting the definition of $\mathbf{H}$ given in eq. (12) into our definition of the variance, eq. (10), and changing the integration to be over $\bar{\mathbf{k}}$ we get

$$\sigma^2(\mathbf{x}) = |\det(\mathbf{V}_u)|\mathbf{b}^{\mathrm{T}}(\mathbf{x})\Bigg\{\iint_{\mathcal{W}_0}\left[\mathbf{H}(\bar{\mathbf{k}}) + \mathbf{D}(\upsilon, \bar{\mathbf{k}})\right]^{-1}\mathbf{\Lambda}^{-1}(\Upsilon_x, \Upsilon_y)\mathbf{C}_{\mathrm{d}} \times \mathbf{\Lambda}^{-1}(\Upsilon_x, \Upsilon_y)\left[\mathbf{H}(\bar{\mathbf{k}}) + \mathbf{D}(\upsilon, \bar{\mathbf{k}})\right]^{-1^{\mathrm{T}^*}} \mathrm{d}^2\bar{\mathbf{k}}\Bigg\}\mathbf{b}(\mathbf{x})^*. \tag{14}$$

Therefore, changing the sample-spacing affects the output variance by changing $\mathbf{H}$ to $\mathbf{H} + \mathbf{D}$ and by replacing the covariance matrix with $\mathbf{\Lambda}^{-1}(\Upsilon_x, \Upsilon_y)\,\mathbf{C}_{\mathrm{d}}\Lambda^{-1}(\Upsilon_x, \Upsilon_y)$. Because $\mathbf{\Lambda}^{-1}$ is diagonal, and because it acts only to change the covariance matrix, its effects on output noise are easy to model. In effect, $\mathbf{\Lambda}^{-1}$ acts to change—relative to the gravity component—the output errors due to gradient measurements. As a

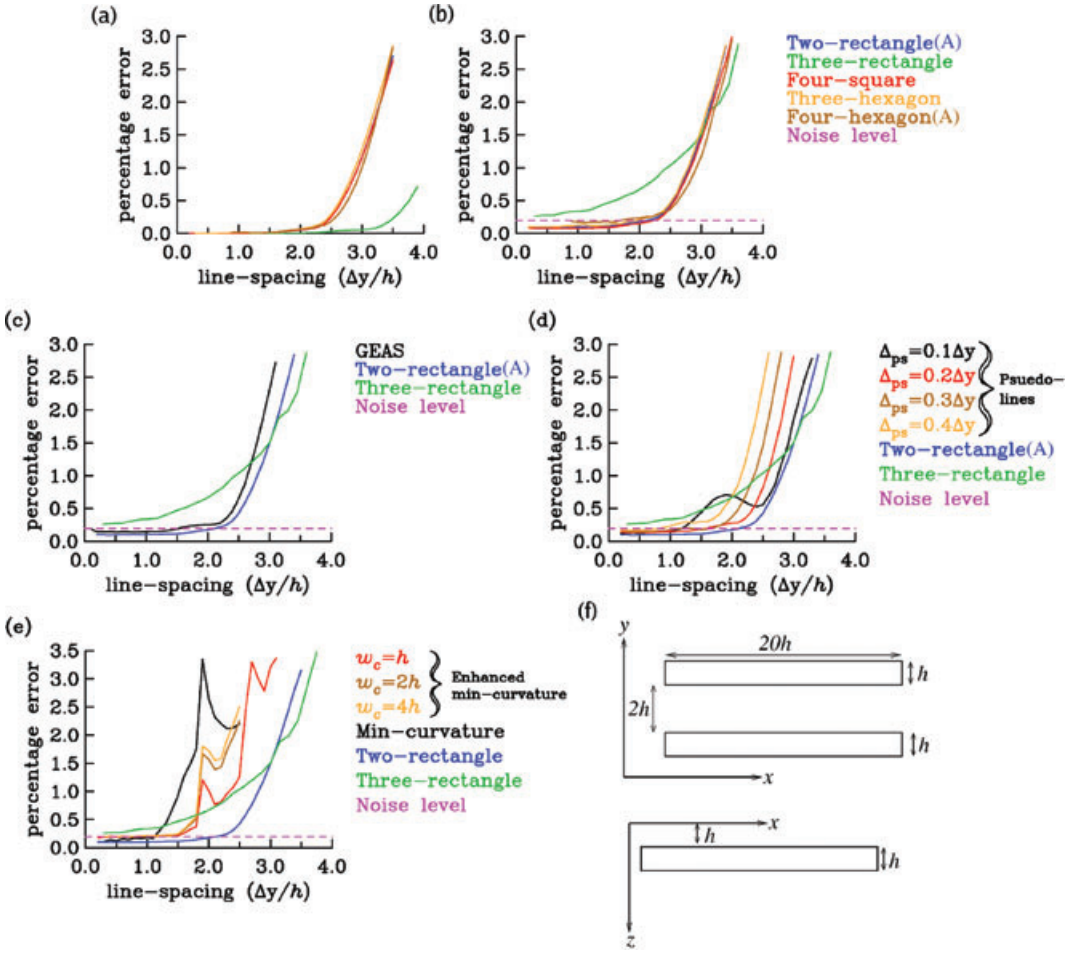

Figure 5. The relationship between line-spacing and output error of the successful expansions. All plots were generated by calculating the percentage output error of the expansions when applied at increasing line-spacings above the twin sources shown in (f). Each line is the average of ten realizations of such an experiment. Plot (a) shows the results without noise added, while plot (b) shows the results when all gradient components are contaminated with 2 per cent (of peak) non-covariant Gaussian noise. The other plots show results obtained with other gradient enhanced interpolation methods: (c) Gradient-Enhanced Akima Splines (GEAS) (Akima 1970); (d) Pseudo-lines (Hardwick 1999), where Δ_{ps} is the distance of the pseudo-lines from the data lines; (e) gradient-enhanced minimum curvature [first described in O'Connell *et al.* (2005); however, the algorithm used here is given more fully in While (2006)], where w_c is a switch over distance between gradient enhanced minimum curvature and normal minimum curvature. The dashed pink line shows the noise level expected with a normal oversampled data set.

simple example, in a Two-rectangle(A) expansion (see WBJ08 for a detailed example using this expansion), where $\Delta y = \Delta x = \Delta$

$$\mathbf{\Lambda}^{-1} = \begin{pmatrix} 1 & 0 \\ 0 & \Delta \end{pmatrix}, \tag{15}$$

where Δ is an arbitrary distance.

To see how line-spacing affects the expansions, Fig. 5 shows how the output error of the expansions changes with line-spacing. Also shown on the figure for comparison are the results obtained by using other gradient enhanced interpolation methods: Akima splines with known gradients (gradient-enhanced Akima splines) (Akima 1970; Marcotte *et al.* 1990; Hardwick 1996), gradient-enhanced minimum-curvature (O'Connell *et al.* 2005), and pseudo-lines (Hardwick 1999). The results shown on the figure were calculated using a twin source experiment, identical to an experiment conducted in WBJ08. In the experiment synthetic surveys of steadily increasing line-spacing were conducted over two long cuboidal sources separated by a distance equal to their depth, as is shown in Fig. 5(f). In the case shown here 2 per cent (of peak) error has been added to all gravity/gradient components. All plots within Fig. 5 show a dramatic increase in noise at some line-spacing. This is simply the aliasing point of each method and, for the expansions in Fig. 5(a), matches up well with the theoretical aliasing points derived in WBJ08 (3× line-spacing for the Three-rectangle expansion, 2× for the Two-rectangle(A) expansion, etc.). However, before this aliasing point each of the expansions and other methods behave differently under the addition of random noise. Most importantly, the Two-rectangle(A), Four-square and Three-hexagon expansions are of lower noise than would be expected conventionally, while the Four-hexagon(A) expansion exhibits approximately the same noise as ordinary sampling. Indeed, the expansions compare well against the other gradient enhanced methods, with the Two-rectangle(A) expansion shown in Figs 5(c)–(e) to have output noise that is up to 0.1 percentage units less than the alternate techniques. This is also true for the Four-square and Three-hexagon expansions, as may be verified by comparing their curves in

Fig. 5(b) to the other plots. Unfortunately the Three-rectangle expansion displays a very large increase in error with increasing line-spacing. Because the other expansions show no similar increase, we can be confident that the shape of the noise curve for the Three-rectangle expansion cannot be simply caused by the gradient error magnification due to $\mathbf{\Lambda}^{-1}$. Instead, the enhanced noise on the Three-rectangle expansion must be due to the increasing distortion of the sampling lattice represented by $\mathbf{D}$. As an aside, this instability under noise, combined with the problems due to edge effects described in WBJ08, render the Three-rectangle expansion unsuitable for practical use.

As discussed in our section on predicted error, reduced noise levels are expected for the Two-rectangle, Four-square, and Three-hexagon expansions, provided errors on the input gradients are sufficiently small; this is the origin of the noise reduction seen in Fig. 5. However, in this section we have shown that gradient errors are amplified by increasing line-spacing, thus we expect there to be a line-spacing where gradient errors dominate. In Fig. 5, noise reduction is seen up until the aliasing point and thus the gravity errors must outweigh the gradient errors until this point. In general this may not always be the case. However, we can estimate for a conventional survey the line-spacing at which gradient errors start to dominate. The exact line-spacing will depend on the expansion used and on the measurement accuracy of the survey, but for a rough estimate let us consider gravity errors of 0.2 mGal (the noise level of a high accuracy airborne gravimeter, Sander *et al.* 2004) and 5 Eötvös errors on the gradients (approximately the accuracy quoted for airborne gradiometers, Murphy 2004; Dransfield & Lee 2004). This being the case, and looking at Fig. 1, the break even point for the Four-square expansion is about 700 m and can be shown to be 1200 m for a Two-rectangle(A) expansion. Both these figures are substantially greater than the decimated line-spacing of the Cannington data discussed in WBJ08 or the real data set discussed below. Thus we can be confident that the criteria for noise reduction in these expansions will often be met in real surveys.

ALONG-LINE CORRELATED NOISE

Airborne or shipborne potential field surveys tend to suffer from levelling errors, whereby individual data lines are beset by long wavelength correlated errors that give a colour map of the data a corrugated appearance. There are a number of methods for dealing with this problem (see, e.g. Urquhart 1988; Minty 1991; Ferraccioli *et al.* 1998; Mauring & Kihle 2006). Regardless, it is likely that some along-line correlated error will always be present in gravity data sets and we would wish the GSE method to be able to deal sensibly with this type of error.

Along-line correlated errors are more difficult to deal with analytically than pure random error. For instance, it has been found empirically that expansions of along-line correlated errors can produce an imaginary output. Therefore, instead of directly calculating the variance as above, the expansion variances were found numerically by applying each expansion to along-line correlated noise and estimating the output variance from the result.

Along-line correlated errors can be modelled as an additional term in eq. (5), so that

$$\tilde{\mathbf{d}}(\mathbf{x}) = \mathbf{d}(\mathbf{x}) + \boldsymbol{\varepsilon}(\mathbf{x}) + \boldsymbol{\varepsilon}^{\mathrm{c}}(\mathbf{x}), \tag{16}$$

where $\boldsymbol{\varepsilon}^{\mathrm{c}}(\mathbf{Vq})$ is a vector of the along-line correlated errors. This is still a linear equation and the effects of along-line correlated noise on the expansions can be isolated from the other terms. Consequently, output noise due to along-line correlated error is simply the expansion of $\varepsilon^{\mathrm{c}}(\mathbf{Vq})$.

In our numerical calculations of expansion error, along-line correlated noise was modelled with the Fourier series

$$\varepsilon^{\mathrm{c}}_p(\mathbf{x}) = \frac{\epsilon^{0\mathrm{c}}_p(y)}{2} + \sum_{j=1}^{\infty} \epsilon^{\mathrm{ac}}_{jp}(y) \sin\left(\frac{2\pi j x}{L}\right) + \epsilon^{\mathrm{bc}}_{jp}(y) \cos\left(\frac{2\pi j x}{L}\right), \tag{17}$$

where $\varepsilon^{\mathrm{c}}_p$ are the components of $\boldsymbol{\varepsilon}^{\boldsymbol{c}}$, L is the length of the data series, and the Fourier coefficients—$\epsilon^{0\mathrm{c}}_p(y)$, $\epsilon^{\mathrm{ac}}_{jp}(y)$ and $\epsilon^{\mathrm{bc}}_{jp}(y)$—are constants in the along-line x direction and stationary stochastic variables in the across-line y direction. The reason for modelling the along-line correlated error using a Fourier series is because it has an easily controlled wavelength parameter $k_{x_{\mathrm{c}}} = \frac{j}{L}$. In real data sets along-line correlated errors tend to be of long-wavelength (Minty 1991), consequently only the first few terms of eq. (17) need be considered.

To model the effects of along-line correlated error, each expansion was tested using synthetic data sets created using eq. (17). For a data set $\frac{\epsilon^{0\mathrm{c}}_p(y)}{2}$, $\epsilon^{\mathrm{ac}}_{jp}(y)$ and $\epsilon^{\mathrm{bc}}_{jp}(y)$ each have, in the cross-line direction, a mean of zero and a variance of one. To calculate the output variance of an expansion we considered only the real part of its output; any imaginary part must be unphysical and can always be discounted. The results of this test are shown in Fig. 6, which plots the output variance against $k_{x_{\mathrm{c}}} \Delta x$. In order to minimize statistical variation, the results presented in the figure are an average of ten realizations of the test conducted over a 256 × 256 sample point grid (rectangular expansions) or a 768 × 256 point grid (hexagonal expansions). The results in the figure are consistent with the results seen for random noise. Most of the expansions shown have an output variance that is for all wavelengths of noise less than the input variance; these expansion can be expected to perform well in the presence of along-line correlated noise. Two expansions, the Three-rectangle and Four-hexagon(D) expansions, have a higher output variance than their input; these expansions can be expected to be poorly behaved in the presence of along-line correlated noise. A further point of interest from the figure is that, over the range of wavenumbers shown, the output variances change very little with the wavelength of the along-line correlated noise. The Three-rectangle expansion variance increases slightly and the Four-square expansion variance decreases slightly, the variances of the other expansions show almost no change. This shows, at least for the long wavelengths of interest, that there is very little dependence of the output variance of the expansions on the wavelength of any along-line correlated noise.

An illustration of the expansion of data contaminated with along-line correlated noise is shown in Fig. 7. In this figure a Four-square expansion is applied to a data set contaminated with along-line correlated noise. The synthetic gravity field used in the figure is identical to

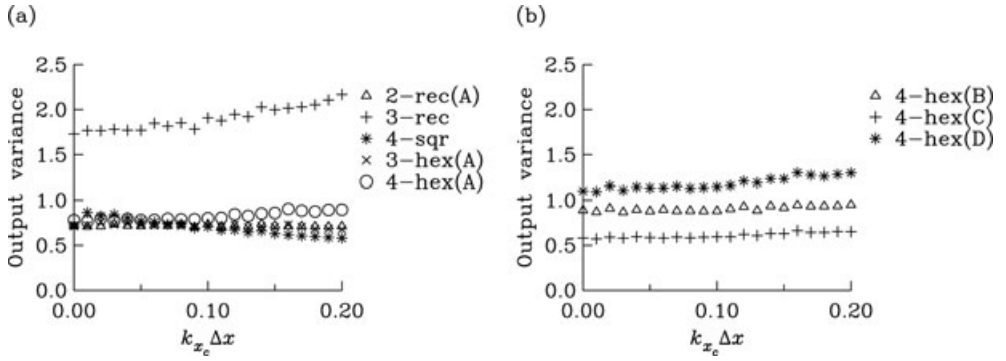

Figure 6. Output variance of expansions contaminated with along-line correlated noise of different wavelengths. The plots show the output variance of the different expansions applied to a data set consisting of along-line correlated errors described by a Fourier series, see text for details. The results shown are an average of ten realizations of the test applied to either a 256 × 256 point grid (rectangular sampling) or a 768 × 256 point grid (hexagonal sampling). Expansions tested are indicated in each plot.

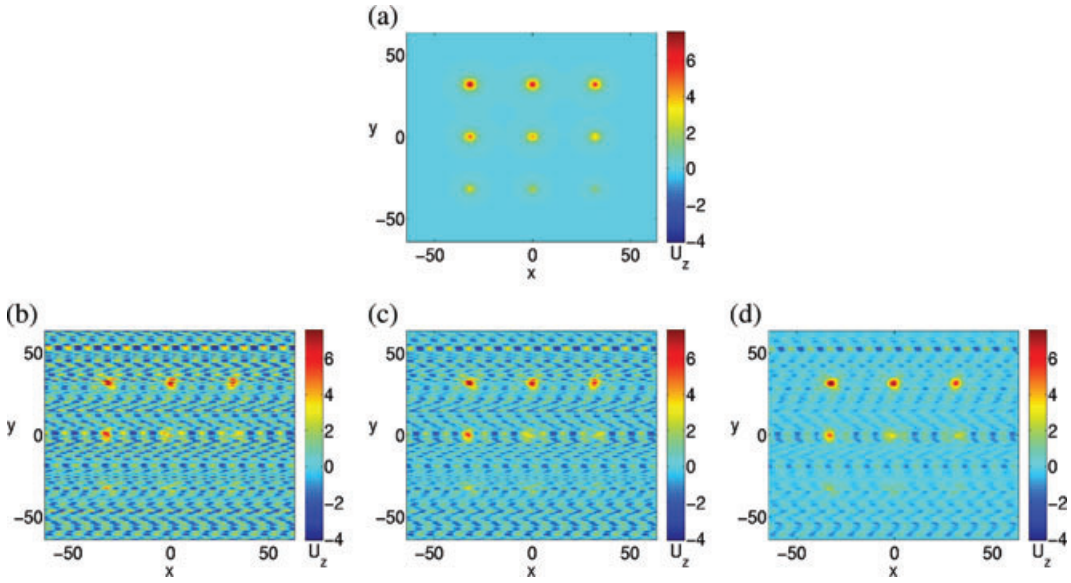

Figure 7. Four-square expansion of a signal contaminated with along-line correlated noise. (a) The test signal: gravity/gradient field of nine points sources of decreasing mass. The amplitude of the peaks decrease in decrements of 10 per cent. (b) Noise contaminated $\tilde{U}_z$ signal; see text for details. (c) Four-square expansion of the noisy signal. (d) The reconstructed signal at the interpolation points of minimum variance (the pink crosses on the diagonal in Fig. 1).

the one used in Figs 3 and 4. For the figure the synthetic data were contaminated by along-line correlated noise of wavenumber $k_{x_c} = 0.1$ and an across-line variance of 20 per cent of the peak amplitude of the relevant gravity/gradient component. The effect of along-line correlated noise on the test function is seen to be substantial and, to the eye, appears worse than the equivalent random error case shown in Fig. 3(b). However, the application of the Four-square expansion reduces this error considerably. This is not true in the along-line x direction; from Fig. 7(c) we can see that along the lines the error appears constant. However, at the interline interpolation points there is a considerable decrease in noise. This decrease is seen in Fig. 7(d) and is quite startling; it is at least as significant as the decrease seen in Fig. 3(d). It should be noted that this behaviour is unlike the random noise case (see Fig. 1) where both along-line and interline interpolation points were of reduced variance.

APPLICATION TO REAL DATA

The theoretical viability of the GSE was demonstrated in WBJ08 and we have shown here that we expect many expansions to be well behaved under the addition of noise. Thus we can fully expect the application of the GSE to real data to produce valuable results. To demonstrate this we present here an example of the GSE applied to a data set collected in the North Sea. The data set is the same data set as described in While *et al.* (2006) and consists of a set of data lines separated by approximately 100 m, a spacing that we assume is sufficient to oversample the gradient field. At each measurement point within the data set, data for all six gravity gradients ($\tilde{U}_{xx}$, $\tilde{U}_{yy}$, $\tilde{U}_{zz}$, $\tilde{U}_{xz}$, $\tilde{U}_{yz}$ and $\tilde{U}_{xy}$) are available; however, there is no equivalent gravity $\tilde{U}_z$ data. As provided to us the data had undergone some post acquisition processing and had been line-levelled. Nonetheless, as the data are subject to both acquisition and processing challenges, we can expect the measured gradients

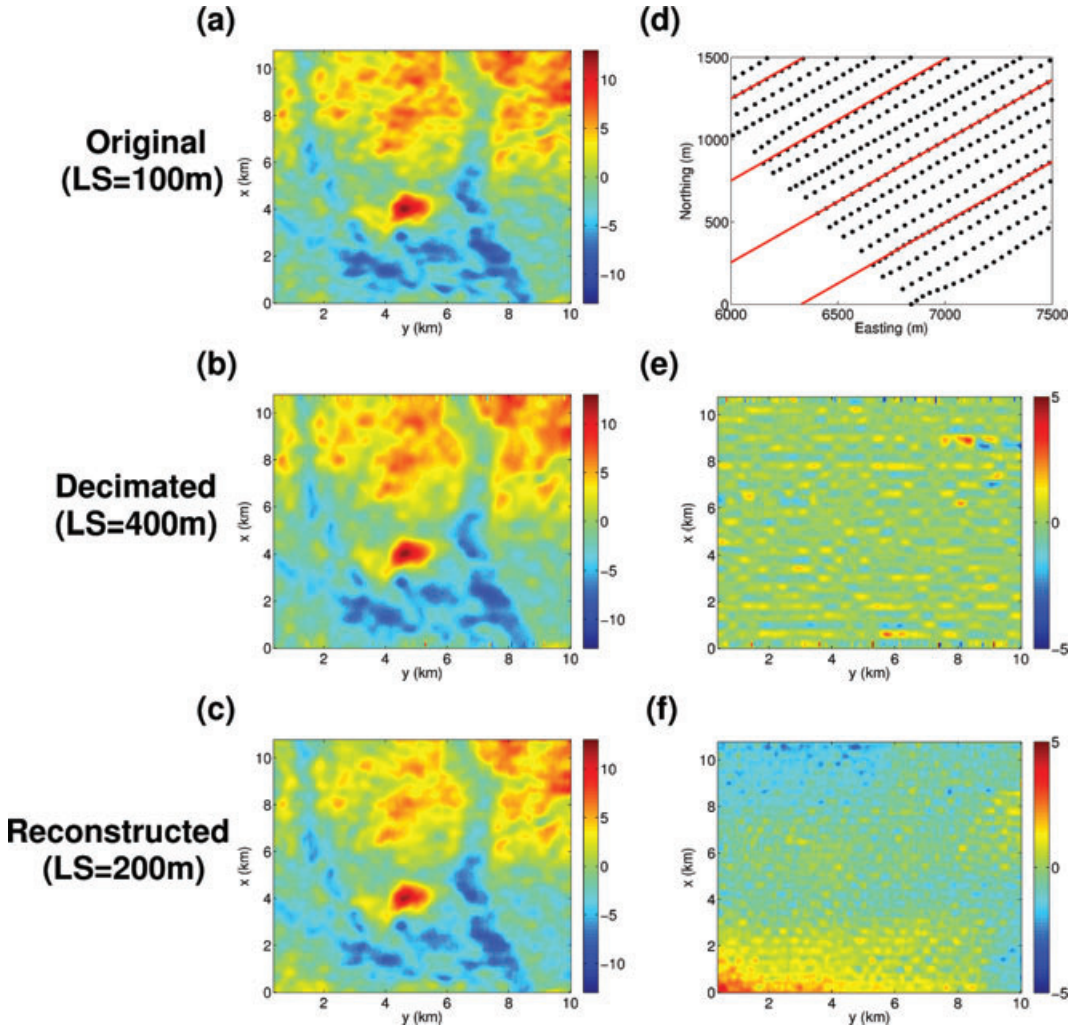

Figure 8. Two-rectangle(c) expansion applied to real data. (a) U_{zz} component of the original data. (b) Data after 3 in 4 data-lines have been removed. (c) Data after reconstruction using the Two-rectangle(C) expansion and filtering to reduce edge effects. (d) Orientation and position of the lines of best fit (shown in red) used to grid the data (black dots); only a small portion of the data extent is shown. (e) Difference between (b) and (a). (f) Difference between (c) and (a). All images have been interpolated to the same resolution using Matlab's cubic interpolator. All gradients are given in Eötvös. LS: line-spacing.

to contain errors from both their initial measurement and subsequent processing. Furthermore, we can expect the errors to have a non-zero correlation length and for their covariance matrix to be non-diagonal. We do stress that the error covariance matrix for the data is not known. An image of the U_{zz} component of the survey can be found in Fig. 8(a).

As we have no measurements of $\tilde{U}_z$, we are limited to expansions that use only gradients as inputs. The Two-rectangle(C) expansion, which uses $\tilde{U}_{zz}$ and $\tilde{U}_{yz}$ to expand for U_{zz}, is one such expansion and is the one performed here. Unfortunately, as can be seen from Table 1, this expansion can be expected to increase any noise present. However, the noise amplification is relatively small (40 per cent or less increase in the noise standard deviation when the covariance matrix is the identity) and is the smallest increase in noise of any permissible expansion. In order to apply the expansion the data need to be evenly spaced both along-line and across-line; unfortunately the measured data deviate slightly from this ideal and must be interpolated onto such a grid. In order to minimize the error induced by this interpolation we first used a linear inversion to find the parameters of the following equation

$$\tilde{y} = m\tilde{x} + c + n\Delta\tilde{y}, \tag{18}$$

where $\tilde{x}$ and $\tilde{y}$ are Easting, and Northing coordinates, m is the gradient of the grid, c is the intercept of the lowest line in the grid, $n = 0, 1, 2, 3, \ldots$ is an integer count of the lines in the Northing direction, and $\Delta\tilde{y} = \Delta y\{\cos[\tan^{-1}(m)]\}$ is the vertical separation of the lines. This equation describes a set of equispaced parallel lines and, after suitable parameters were inverted for, can be seen in Fig. 8(d) to match the lie of the data closely. We gridded the data onto these lines using nearest neighbour interpolation and then tensor rotated (Riley *et al.* 2004, chap. 21) the data into an along-line x, across-line y coordinate system.

To test the expansion on the gridded/rotated data we first decimated the data by omitting 3 out of every 4 data lines, leaving a data set, the decimated data set, containing 28 lines with a line-spacing of 400 m. Then, after removing the means from all gradient components, we applied the expansion for U_{zz} to the data giving a data set with a line-spacing of 200 m. Following WBJ08, we further processed this data set

by filtering with a 500 m wavelength eighth-order Butterworth filter in order to reduce edge-effect errors. This final data set, the reconstructed data set, and the decimated data set were then interpolated using cubic interpolation to a 100 m line-spacing and compared to the original data.

The results of this test can be seen in Fig. 8. It is immediately apparent that the expansion has recreated a reasonable approximation of the oversampled signal. More detail is obtained by looking at the difference plots of Figs 8(e) and (f). Here it can be seen that the reconstructed data set has significant deficiencies at its top and bottom edges that are almost certainly due to residual edge effects. These errors tend to dominate and result in an rms value of plot (f) of 0.88 E (1 E=1 Eötvös $= 10^{-9}\,\mathrm{s}^{-2}$) which is high compared to an rms of 0.55 E for plot (e). However if we omit the bottom and top edges of the data series then the expansion performs much better. In this case the rms values of plots (e) and (f) are almost identical [0.49 E for plot (f) and 0.48 E for plot (e), when calculated between 3 and 8 km in the y direction]. However, this is not the complete picture; it is evident from looking at the plots that in some regions the decimated data does much worse than the reconstructed data. It is in these regions that the 400 m line-spacing is not adequate to resolve the U_{zz} field and only by applying the expansion can we get near the truth.

What appears to have occurred in this real data test is that edge effects and the inherent noise amplification of the expansion has raised the noise level in the reconstructed data from that of the decimated data. However, this is offset in regions where the decimated data are of insufficient density to resolve the U_{zz} field while the expansion can still resolve the truth. In this test these two competing effects, in the mid-portions of the data set at least, have largely offset each other. It should be remembered that this is a harsh test of the GSE as we have been forced to use an error increasing expansion and have used data of extremely limited extent. Nonetheless the expansion has produced reasonable results, has not excessively amplified the error, and has substantially reduced errors due to undersampling. Furthermore, it is to be expected that superior results would have been obtained if the data set had been of greater extent, and/or an expansion that was noise reducing was used.

DISCUSSION AND CONCLUSIONS

It is shown in WBJ08 that the GSE is a method for combining undersampled gravity/gravity gradient (or, equally applicable, magnetic and magnetic gradient) measurements into an over-sampled data set. It has been the purpose of this paper to show that the GSE has predictable noise propagation characteristics and to examine these characteristics for some of the more important types of expansion. Unfortunately, it has been shown that many expansions will always enhance any noise present in their input data. However, many key expansions, such as the Two-rectangle(A) and Four-square expansions, are shown to be well behaved in the presence of noise. In fact, in our numerical experiments the noise propagation properties of these expansions appear to be superior to that of other gradient enhanced interpolation methods. Furthermore, if the line spacing is not too large and the noise on the gradient components is small compared with the gravity noise, then the output from these 'good' expansions will often be less noisy than that of the original data. Such properties appear to be true for both random stochastic error and along-line correlated error.

Although consideration must be taken of edge effects and non-band limited signal (discussed in WBJ08), it has, nevertheless, been shown that measurement error need not be a significant worry in our GSE method. It is therefore safe to conclude that the best expansions, particularly the Two-rectangle(A) and Four-square expansions, can be applied to real data sets without worry that measurement error will invalidate the result.

We have also demonstrated for the first time the application of the GSE to a set of real data. In what was a harsh test, the Two-rectangle(C) expansion was carried out on a deliberately undersampled data set. Over much of the domain of interest the expansion, despite edge effects and the noise enhancing properties of the expansion used, produced results comparable to normal interpolation. In addition, the expansion was able to reduce errors due to undersampling of the data. This demonstrates that the GSE is a viable method for the reduction of sampling error in regions of sparse data even when the data are noisy.

ACKNOWLEDGMENTS

This work was funded by a NERC CASE studentship with Shell Expro.

REFERENCES

Akima, H., 1970. A new method of interpolation and smooth curve fitting based on local procedures, *J. Assoc. Comput. Mach.,* **17,** 589–602.

Bell, R.E., Anderson, R. & Pratson, L., 1997. Gravity gradiometry resurfaces, *Leading Edge.,* **16,** 55–60.

Brown, J.L. Jr, & Cabrera, S.D., 1990. Multi-channel signal reconstruction using noisy samples, in *Proceedings of the IEEE International Conference on Acoustics, Speech, and Signal Processing, Expanded Abstracts,* pp. 1233–1236, IEEE.

Brown, J.L. Jr, & Cabrera, S.D., 1991. On well-posedness of the Papoulis generalized sampling expansion, *IEEE Trans. Circuits Syst.,* **38,** 454–456.

Cheung, K.F. & Marks, R.J. II, 1985. Ill-posed sampling theorems, *IEEE Trans. Circuits Syst.,* **32,** 481–484.

Cheung, K.F., Poon, M.C. & Marks, R.J. II, 1989. A multidimensional extension of Papoulis' generalized sampling expansion and some of its applications, in *International Symposium on Computer Architecture and Digital Signal Processing, Expanded Abstracts,* pp. 267–271, Inst. Electronic Engineers.

Dransfield, M.H. & Lee, J.B., 2004. The FALCON airborne gravity gradiometer survey systems, in *Abstracts from the ASEG-PESA Airborne Gravity 2004 Workshop,* pp. 15–19.

Droujinine, A., Vasilevsky, A. & Evans, R., 2007. Feasibility of using full tensor gradient (FTG) data for detection of local lateral density contrasts during reservoir monitoring, *Geophys. J. Int.,* **169,** 795–820.

Ferraccioli, F., Gambetta, M. & Bozzo, E., 1998. Microlevelling procedures applied to regional aeromagnetic data: an example from the transantarctic mountains, *Geophys. Prospect.,* **46,** 5–11.

FitzGerald, D.J. & Holstein, H., 2006. Innovative data processing methods for gradient airborne geophysical data sets, *Leading Edge,* **25,** 87–94.

Hardwick, C.D., 1996. Aeromagnetic gradiometry in 1995, *Expl. Geophys.,* **27,** 1–11.

Hardwick, C.D., 1999. Gradient-enhanced total field gridding, in *SEG, Expanded Abstracts,* pp. 381–384, SEG, Tulsa, OK.

Lee, J.B., 2001. FALCON gravity gradiometer technology, *Expl. Geophys.,* **32,** 247–250.

Marcotte, D.L., Hardwick, C.D. & O'Connel', M., 1990. Aeromagnetic gradiometry methods: a study using real data, in *SEG, Expanded Abstracts,* pp. 584–586, SEG, Tulsa, OK.

Mauring, E. & Kihle, O., 2006. Levelling aerogeophysical data using a moving differential median filter, *Geophysics,* **71,** 5–11.

Mikhailov, V., Pajot, G., Diament, M. & Price, P., 2007. Tensor deconvolution: a method to locate equivalent sources from full tensor gravity data, *Geophysics,* **72,** I61–I69.

Minty, R.R.S., 1991. Simple micro-levelling for aeromagnetic data, *Expl. Geophys.,* **24,** 115–116.

Murphy, C.A., 2004. The air-FTG airborne gravity gradiometer system, in *Abstracts from the ASEG-PESA Airborne Gravity 2004 Workshop, Geoscience Australia Record 2004/18,* pp. 7–14, ed. Lane, R., Available at www.bellgeo.com, accessed on 2006 November 3.

O'Connell, M.D., Smith, R.S. & Vallée, M.A., 2005. Gridding aeromagnetic data using longitudinal and transverse horizontal gradients with the minimum curvature operator, *Leading Edge.,* **24,** 142–145.

Pajot, G., Viron, O., Diament, M., Lequentrec-Lalancette, M.-F. & Mikhailov, V., 2008. Noise reduction through joint processing of gravity and gravity gradient data, *Geophysics,* **73,** I23.

Papoulis, A., 1977. Generalized sampling expansion, *IEEE Trans. Circuits Syst.,* **24,** 652–654.

Pratson, L.F. et al., 1998. Results from a high-resolution, 3-D marine gravity gradiometry survey over a buried salt structure, Mississippi canyon area, Gulf of Mexico, in *SEG Geophys Ref. Series 8, AAPG Studies in Geology,*Vol. 43, pp. 137–145.

Riley, K.F., Hobson, M.P. & Bence, S.J., 2004. *Mathematical Methods for Physics and Engineering,* 2nd edn, Cambridge University Press.

Sander, S., Argyle, M., Elieff, S., Ferguson, S., Lavoie, V. & Sander, L., 2004. The AIRGrav airborne gravity system, in *Abstracts from the ASEG-PESA Airborne Gravity 2004 Workshop,* pp. 15–19.

Seidner, D. & Feder, M., 1998. Noise sensitivity of GSE systems, in *Proceedings of the 8th Digital Signal Processing workshop,* pp. 584–586.

Seidner, D. & Feder, M., 1999. Optimal generalized sampling expansion, in *Proceedings of tthe IEEE International Conference on Acoustics, Speech, and Signal Processing, Expanded Abstracts,* pp. 1637–1640, IEEE.

Urquhart, T., 1988. Decorrugation of enhanced magnetic field maps, in *Proceedings of the 58th SEG Annual International Conference and Exhibition, Expanded Abstracts,* pp. 371–372, SEG, Tulsa, OK.

Vasco, D.W., 1989. Resolution and variance operators of gravity and gravity gradiometry, *Geophysics,* **54,** 889–899.

Vasco, D.W. & Taylor, C., 1991. Inversion of airborne gravity gradient data, southwestern Oklahoma, *Geophysics,* **56,** 90–101.

While, J., 2006. Spectral methods in gravity gradiometry, *PhD thesis*, University of Leeds.

While, J., Jackson, A., Smit, D. & Biegert, E., 2006. Spectral analysis of gravity gradiometry profiles, *Geophysics,* **71,** J11.

While, J., Biegert, E. & Jackson, A., 2008. Interpolation of gravity and gravity gradient data by using the generalized sampling expansion: theory, *Geophysics,* **73,** I11–I21.

Zhdanov, M.S., Ellis, R. & Mukherjee, S., 2004. Three-dimensional regularized focusing inversion of gravity gradient tensor component data, *Geophysics,* **69,** 925–937.